

Enol Formation and Ring-Opening in OH-Initiated Oxidation of Cycloalkenes

Giovanni Meloni*

Department of Chemistry, University of San Francisco, San Francisco, California 94117

Talitha M. Selby, David L. Osborn, and Craig A. Taatjes*

Combustion Research Facility, Mail Stop 9055, Sandia National Laboratories, Livermore, California 94551-0969

Received: September 9, 2008; Revised Manuscript Received: October 22, 2008

Photolytic OH-initiated oxidation of cyclopentene, cyclohexene, and 1,4-cyclohexadiene have been investigated by using tunable synchrotron photoionization mass spectrometry. Electronic structure calculations (CBS-QB3) are employed in Franck–Condon (FC) spectral simulations of the photoionization efficiency curves (PIE) of the observed products. Cyclopentenol (cyclopenten-1-ol, 1-*c*-C₅H₇OH) and its isomers cyclopenten-2-ol (2-*c*-C₅H₇OH) and cyclopentanone (*c*-C₅H₈=O), are detected from OH-initiated cyclopentene oxidation. The measured adiabatic ionization energy (AIE) of 1-*c*-C₅H₇OH is 8.4(±0.1) eV, and that of 2-*c*-C₅H₇OH is 9.5(±0.1) eV. The calculated AIE of possible cyclopentene oxidation products *cis*-1,2-epoxycyclopentane and 2,3-epoxycyclopentanol is 9.97 and 9.44 eV, respectively. Product spectra from OH-initiated oxidation of cyclohexene and cyclohexa-1,4-diene show a substantial contribution from linear aldehydes, indicating a prominent role for ring opening. Implications for the oxidation chemistry of cycloalkenes are briefly discussed.

Introduction

Oxidation in combustion systems,^{1,2} in the stratosphere, and in the troposphere³ is often initiated by reaction of the hydroxyl radical. In general, the main reaction channel for reactions with alkenes is the addition of OH to the double bond, with a minor channel due to hydrogen abstraction.⁴ Specific attention has recently been devoted to cyclopentene reactions,^{5,6} because of high sooting tendency in cyclopentene combustion,^{7,8} and because of cyclopentene's possible role in the formation of secondary aerosol particles.⁹ In fact, it has been shown that the photochemical degradation of cyclopentene, and cyclic alkenes in general, by ozone and hydroxyl radicals first yields glutaraldehyde, which can undergo further oxidation to form glutaric acid and other oxygenated species¹⁰ that account for much of the organic fraction of suspended particulate matter.

Moreover, it has been suggested that reactions of alkenes with OH, and the OH-initiated oxidation of alkenes, may form enols. The presence of enols in many flames has been demonstrated by using a molecular beam mass spectrometric technique coupled with tunable vacuum ultraviolet (VUV) light.¹¹ Ethenol (vinyl alcohol) has also recently been detected in the interstellar medium by means of its microwave spectrum.¹² It has also been proposed that oxidation of enols may contribute to organic acid formation in the troposphere.¹³ The first gas phase identification of the simplest enol, ethenol, was accomplished only in 1976 by Saito¹⁴ using microwave spectroscopy. From the rotational analysis he demonstrated that the *syn* conformer is the more stable, and also confirmed that gas-phase ethenol is a stable molecule.¹⁵ On the other hand, the ethenol cation has its lowest energy configuration with the hydroxyl group in the *anti* position,^{16,17} which gives relatively small Franck–Condon factors for the adiabatic ionization transition of vinyl alcohol.¹⁸

Finally, the oxidation of cyclic alkenes is an important intermediate step in the oxidation of the naphthenic (cycloalkane) compounds that are increasingly important components in the motor fuel stream, especially in parts of North America where oil-sands derived fuels are prominent. The ignition and low-temperature oxidation chemistry of these compounds remain poorly characterized despite a recent increase in interest.

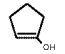
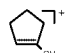
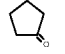
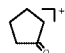
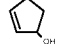
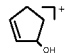
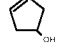
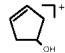


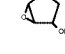
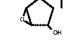
In a continuing effort to characterize photoionization detection of important combustion and atmospheric intermediates, this work reports the photoionization efficiency (PIE) curve of cyclopenten-1-ol (1-*c*-C₅H₇OH) and two other isomers, cyclopentanone (*c*-C₅H₈=O) and cyclopenten-2-ol (2-*c*-C₅H₇OH), and determines adiabatic ionization energies, atomization enthalpies, and enthalpies of formation by a combination of the experimental data with quantum chemical calculations. Furthermore, the OH-initiated oxidation chemistry of cyclopentene is compared with that of the six-membered counterparts cyclohexene and 1,4-cyclohexadiene, which exhibit a prominent contribution from ring-opening to form hex-5-enal in the case of cyclohexene and hex-3,5-dienal and hex-4,5-dienal from 1,4-cyclohexadiene.

Experimental Section

The experiments were carried out at the Chemical Dynamics Beamline of the Advanced Light Source at Lawrence Berkeley National Laboratory, using a multiplexed photoionization time-resolved mass spectrometer, which allows simultaneous probing of the formation and depletion of multiple species during photolytically initiated reactions. Details of the experimental apparatus are presented in a separate publication.¹⁹ Briefly, the apparatus consists of a 60 cm long quartz slow-flow reactor, through which helium, excess reactant, and a precursor flow. The reactions are photolytically initiated, and the chemical species effuse through a 650 μm pinhole into a differentially pumped region, where they are ionized by the tunable VUV radiation of the Advanced Light Source. Ions are then acceler-

* Authors to whom correspondence should be addressed. E-mail: gmeloni@usfca.edu (G.M.); cataatj@sandia.gov (C.A.T.).

TABLE 1: C₅H₈O Isomers and C₅H₈O₂ Product Considered in This Work^c

Molecule	r_{C-C}	r_{C-O}	Energy ^a	$\langle S^2 \rangle$	$\Delta_{at}H_0^\circ$	$\Delta_fH_0^\circ$	$H_{298}^\circ - H_0^\circ$
\tilde{X}^1A 	1.34	1.36	0	-	5647	-116	17.4
\tilde{X}^2A 	1.42	1.30	8.32	0.753	4844	687	17.6
\tilde{X}^1A 	1.53 ^b	1.20	0	-	5697	-166	17.2
\tilde{X}^2A 	1.56 ^b	1.18	9.29	0.756	4800	731	17.9
\tilde{X}^1A 	1.33	1.43	0	-	5631	-100	17.5
\tilde{X}^2A 	1.38	1.37	9.39	0.753	4725	806	18.5
\tilde{X}^1A 	1.33	1.42	0	-	5631	-100	17.6
\tilde{X}^2A 	1.41	1.41	9.17	0.752	4746	785	19.0
\tilde{X}^1A 	1.46 ^b	1.44	0	-	5598	-67	17.5
\tilde{X}^2A 	1.47 ^b	1.44	9.97	0.754	4636	895	18.0
\tilde{X}^1A 	1.52 ^b	1.41	0	-	6011	-233	18.5
\tilde{X}^2A 	1.75 ^b	1.34	9.44	0.754	5099	679	19.6
\tilde{X}^1A CH ₂ =CH-(CH ₂) ₂ CHO	1.51 ^b	1.20	0	-	5604	-73	21.3
\tilde{X}^2A CH ₂ =CH-(CH ₂) ₂ CHO ⁺	1.55 ^b	1.18	9.76	0.759	4663	868	21.8

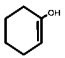
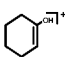
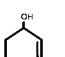
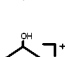
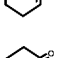
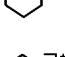
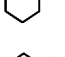


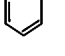
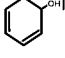
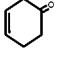
^a The total electronic energies are zero-point energy corrected. ^b This is the C_α-C bond length. ^c B3LYP/6-311+G** optimized bond distances in angstroms and angles in degrees. CBS-QB3 energies, in eV, are relative to the neutral ground electronic state. The atomization enthalpy ($\Delta_{at}H_0^\circ$), the enthalpy of formation ($\Delta_fH_0^\circ$), and the heat content functions ($H_{298}^\circ - H_0^\circ$) are in kJ mol⁻¹.

ated, focused, and mass selected in a double-focusing time-resolved mass spectrometer of the Mattauch-Herzog geometry.²⁰ Finally, the ions hit the active area of a time- and position-sensitive microchannel plate detector with a delay-line anode.²¹ In the present investigation, the photolytic precursor is H₂O₂ that has been generated by thermal decomposition of urea-hydrogen peroxide adduct (97%) kept in a 45 °C thermostated bubbler. The 248 nm KrF excimer laser photolysis of H₂O₂ produces OH radicals that react with cyclopentene (>96%) to form a number of possible products.²² Subsequent reaction with oxygen (present at approximately 10¹³ cm⁻³ from the H₂O₂ source) is also possible. The VUV radiation of the Advanced Light Source can be scanned during an acquisition yielding time-resolved mass spectra at each photon energy. For each acquisition a three-dimensional data block is recorded containing ion intensity as a function of mass-to-charge ratio, reaction time, and photon energy. The experimental photoionization efficiency curve is then obtained by integrating the data over the selected mass-to-charge ratio and time window corresponding to the production of the species of interest. The PIE spectrum signal is background subtracted and normalized for the ALS photon flux at each photon energy.

Computation

To reproduce the overall shape and onset of the PIE curves, a spectral simulation within the Franck-Condon (FC) approximation is performed by using calculated molecular parameters. Electronic structure calculations of 1-*c*-C₅H₇OH, *c*-C₅H₈=O, 2-*c*-C₅H₇OH, cyclohexen-1-ol (1-*c*-C₆H₉OH), cyclohexen-2-ol (2-*c*-C₆H₉OH), cyclohexanone (*c*-C₆H₁₀=O), cyclohexa-1,4-dienol (1,4-*c*-C₆H₇OH), cyclohexa-2,4-dienol (2,4-*c*-C₆H₇OH), hexa-3,5-dienal (CH₂=CH-CH=CH-CH₂CHO), cyclohexen-3-one (3-*c*-C₆H₈=O), and hexa-4,5-dienal (CH₂=C=CH-CH₂-CH₂-CHO) for both the neutral and cation are carried out with use of the Gaussian03 program package.²³ Bond distances, harmonic vibrational frequencies, and force constants are optimized at the Becke three-parameter exchange functional with the Lee, Yang, and Parr correlation functional (B3LYP) level of theory and all electron 6-311+G** basis set. The composite method CBS-QB3^{24,25} is utilized to obtain reliable energetics.²⁵ The optimized geometries and energetics of the three C₅H₈O isomers together with other pertinent species are presented in Table 1. The optimized geometries and energetics for the OH oxidation products of cyclohexene and 1,4-cyclohexadiene are presented in Table 2.

TABLE 2: C₆H₈O and C₆H₁₀O Isomers Considered in This Work^c

Molecule	$r_{C=C}$	$r_{C_\alpha-O}$	Energy ^a	$\langle S^2 \rangle$	$\Delta_{ai}H_0^\circ$	$\Delta_fH_0^\circ$	$H_{298}^\circ - H_0^\circ$
\tilde{X}^1A 	1.34	1.37	0	-	6826	-152	19.8
\tilde{X}^2A 	1.42	1.30	8.26	0.753	6029	645	20.1
\tilde{X}^1A 	1.33	1.43	0	-	6803	-129	20.2
\tilde{X}^2A 	1.39	1.39	9.10	0.753	5925	749	21.2
\tilde{X}^1A 	1.52 ^b	1.21	0	-	6867	-193	19.7
\tilde{X}^2A 	1.56 ^b	1.18	9.19	0.755	5980	694	20.8
\tilde{X}^1A 	1.33	1.37	0	-	6288	-46	19.1
\tilde{X}^2A 	1.40	1.31	8.37	0.753	5479	763	19.3
\tilde{X}^1A 	1.33	1.42	0	-	6264	-22	19.4
\tilde{X}^2A 	1.38	1.39	8.41	0.759	5452	790	19.7
\tilde{X}^1A 	1.33	1.20	0	-	6322	-80	19.1
\tilde{X}^2A 	1.37	1.18	9.02	0.755	5452	790	19.6
\tilde{X}^1A CH ₂ =CH-CH=CH-CH ₂ CHO	1.52 ^b	1.20	0	-	6235	7	23.4
\tilde{X}^2A CH ₂ =CH-CH=CH-CH ₂ CHO ⁺	1.59 ^b	1.18	8.79	0.764	5384	858	23.9
\tilde{X}^1A CH ₂ =C=CH-CH ₂ -CH ₂ -CHO	1.51 ^b	1.20	0	-	6178	64	23.8
\tilde{X}^2A CH ₂ =C=CH-CH ₂ -CH ₂ -CHO ⁺	1.54 ^b	1.19	9.28	0.755	5283	959	24.3

^a The total electronic energies are zero-point energy corrected. ^b This is the C_α-C bond length. ^c B3LYP/6-311+G** optimized bond distances in angstroms and angles in degrees. CBS-QB3 energies, in eV, are relative to the neutral ground electronic state. The atomization enthalpy, the enthalpy of formation, and the heat content functions are in kJ mol⁻¹.

The expectation value of S^2 shows that there is negligible spin contamination. All the vibrational frequencies are real, indicating that the optimized geometries represent minima in the potential energy surface. There are no experimental investigations of the cyclic enols and unsaturated alcohols, 1-*c*-C₅H₇OH, 2-*c*-C₅H₇OH, 1-*c*-C₆H₉OH, 2-*c*-C₆H₉OH, 1,4-*c*-C₆H₇OH, and 2,4-*c*-C₆H₇OH. To assess the accuracy of the optimized geometries needed for the PIE spectral simulation quantum chemical calculations were performed at the same level of theory on the keto isomer of 1-*c*-C₅H₇OH, i.e., cyclopentanone, which has been experimentally investigated. Durig et al.²⁶ recorded the IR and Raman spectra of cyclopentanone, measuring 6 bending modes, 5 in the liquid and 1 in the gas phase. The computed vibrational frequencies of 706 (skeletal bending), 587 (in-plane ring bending), 471 (carbonyl bending),

451 (carbonyl bending), 234 (out-of-plane ring deformation bending), and 96 cm⁻¹ (out-of-plane ring deformation bending) agree very well with the experimental fundamental modes of 711, 583, 472, 450, 236, and 95 cm⁻¹, respectively.²⁶ Also, the calculated rotational constants at the optimized geometry are in excellent agreement with the experimental values obtained from Erlandsson's microwave rotational spectrum,²⁷ with a deviation less than 1%. The computed AIE of 9.29 eV closely matches the experimental value of 9.26(±0.01) eV.²⁸

Results and Discussion

Cyclopentene Oxidation. The photoionization efficiency curve of *m/z* 84 (C₅H₈O) is presented in Figures 1 and 2. It exhibits a gradual onset at around 8.4 eV, a second feature at 9.25 eV, and a third one at 9.4 eV with a steeper threshold.

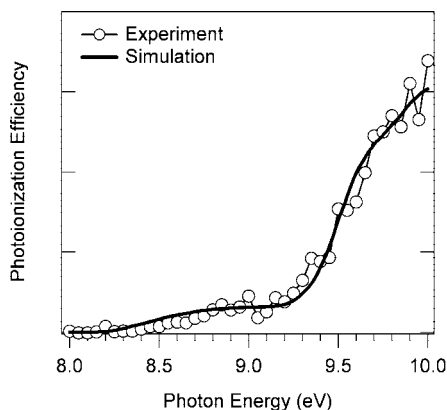


Figure 1. The best-fit overall Franck–Condon PIE curve (solid line) superimposed on the experimental PIE curve of m/z 84 isomers (C_5H_8O).

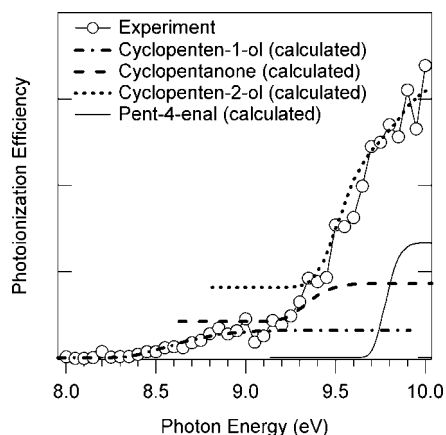


Figure 2. Schematic decomposition of the best fit to the experimental photoionization efficiency spectrum into the substituent calculated photoionization efficiency curves of the three isomers: 1- c - C_5H_7OH , c - $C_5H_8=O$, and 2- c - C_5H_7OH . The isomeric photoionization efficiency curves are scaled by their weighting in the fit to the overall spectrum (see Figure 1) and vertically displaced for clarity. The photoionization efficiency spectrum of pent-4-enal is shown for reference; no evidence of its formation is seen and it is not included in the fit.

The analysis of these data is achieved by a Franck–Condon spectral simulation, using the calculated optimized geometries and force constants for both the neutral and cation electronic states of the three isomers. The simulated FC PIE curve is obtained by computation and integration of the photoelectron spectra at a temperature of 300 K, using the PESCAL program,^{29,30} within the Franck–Condon approximation and including the Duschinsky rotation.³¹ The fit is optimized by varying the ionization energies of the isomers considered for the simulation and the ratio of their integrated signals (see below). The calculated FC overall PIE curve is shown in Figure 1, superimposed on the experimental curve, whereas Figure 2 shows the individual calculated PIE curve of the isomers, superimposed on the experimental data. Contributions from two other possible isomers, *cis*-1,2-epoxycyclopentane, a feasible product of cyclopentene oxidation, and 3- c - C_5H_7OH (cyclopenten-3-ol) can be ruled out. The *cis*-1,2-epoxycyclopentane can be eliminated based on its calculated ionization energy of 9.97 eV. The cyclopenten-3-ol species has a calculated ionization energy of 9.17 eV, but is not included because the reaction system is unlikely to produce this isomer. Rather, the addition of OH to the double bond creates a hydroxycyclopentyl radical, with an unpaired electron localized on the other C sp^2 , which can eliminate an H atom (either directly or via addition of O_2

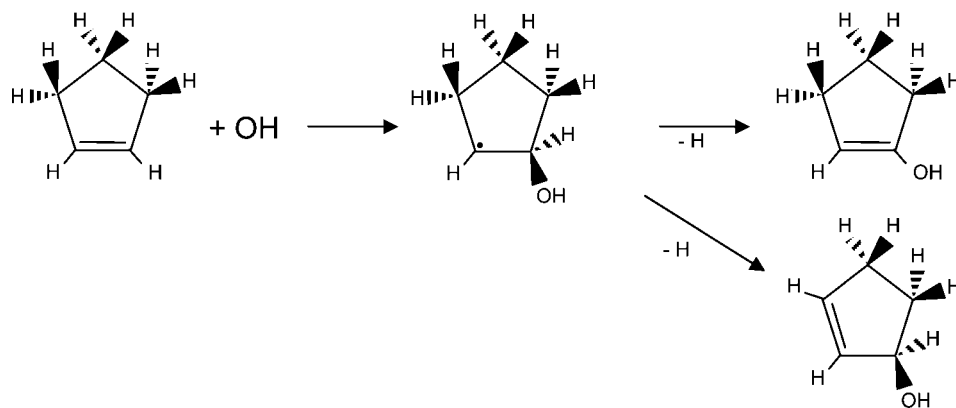
and elimination of HO_2) from either C atom adjacent to the C sp^2 radical center, forming a double bond to give either cyclopenten-1-ol or cyclopenten-2-ol according to the proposed reaction shown in Scheme 1. On the basis of the CBS-QB3 energetics and the FC PIE best fit the observed features can be assigned to the \tilde{X}^+ (cation) + $e^- \leftarrow \tilde{X}$ (neutral) electronic transitions of the three isomers, 1- c - C_5H_7OH , c - $C_5H_8=O$, and 2- c - C_5H_7OH , respectively. For the ground state-to-ground state transitions, the most FC active vibrational modes are used in the simulation, i.e., those modes associated with the larger normal mode displacements. Specifically, 6 modes are used for 1- c - C_5H_7OH , 3 modes for c - $C_5H_8=O$, and 8 modes for 2- c - C_5H_7OH . The most FC active vibrational modes are the $C_{\alpha}=C$ stretching for 1- c - C_5H_7OH , the in-phase CH_2 rock for c - $C_5H_8=O$, and the OH wag for 2- c - C_5H_7OH . The electronic transition from the ground state of the neutral to the ground state of the cation defines the adiabatic ionization energy (AIE).

Because correlations among parameters limit the precision of values derived from a fit to the entire curve, the AIE for 1- c - C_5H_7OH is best derived from a fit to the threshold region (photon energy ≤ 8.9 eV) of the signal, giving $8.42(\pm 0.09)$ eV (calculated 8.32 eV). Fitting the entire curve gives an AIE for 2- c - C_5H_7OH of $9.53(\pm 0.06)$ eV (calculated 9.39 eV). The error limits given are the 95% uncertainty bounds of the fit. The AIE and amplitude of the 2- c - C_5H_7OH are somewhat correlated with those of the other isomers because its threshold is masked by the envelope of the lower energy transitions. This is shown in Figure 2, where the three electronic transitions are plotted separately. The total uncertainty of the reported AIE, $8.4(\pm 0.1)$ eV for 1- c - C_5H_7OH and $9.5(\pm 0.1)$ eV for 2- c - C_5H_7OH , includes factors such as the photon energy calibration, possible presence of hot bands, and the approximate nature of the Franck–Condon factors.

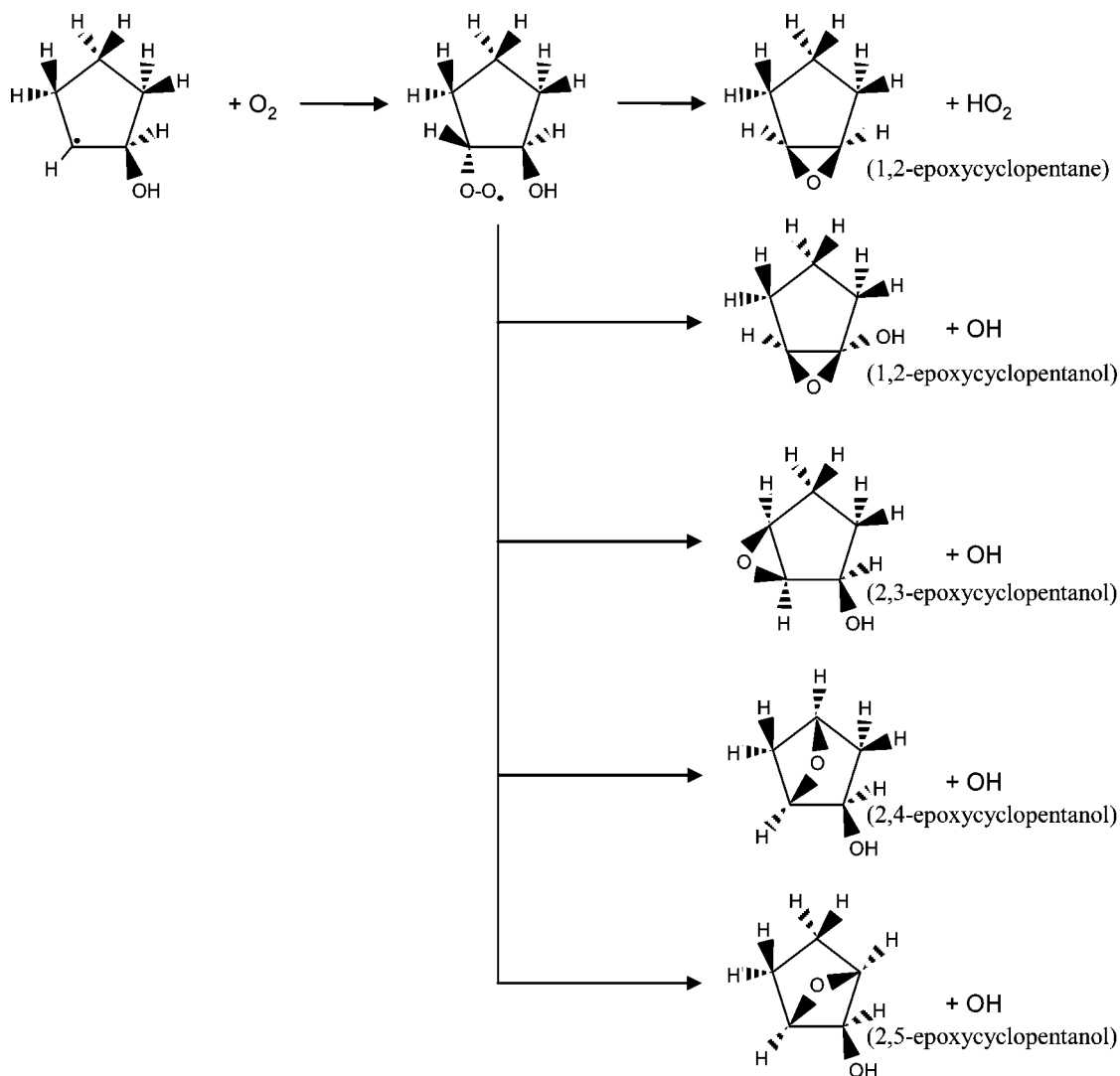
The relative amplitudes of the isomeric contributions require knowledge of the relative photoionization cross sections. From the empirical model of Bobeldijk et al.³² the photoionization cross sections of the three isomers would be expected to be essentially identical at 11.8 eV, well above the region where the Franck–Condon envelope has leveled off. Scaling the fitted contributions using these cross section estimates gives relative isomeric contributions of 1- c - C_5H_7OH : c - $C_5H_8=O$:2- c - C_5H_7OH = $1:1.4(\pm 1):9(\pm 3)$, where the estimated uncertainties are a combination of the 95% uncertainty bounds to the fit and the $\sim 20\%$ uncertainty in the relative cross section estimates.

It is also possible to calculate the atomization enthalpies at 0 K ($\Delta_{at}H_0^\circ$) or binding energies, defined as the enthalpy for the reaction $C_xH_yO_{(g)} \rightarrow xC_{(g)} + yH_{(g)} + O_{(g)}$, of all the species reported in Table 1, using the simple relation $\Delta_{at}H_0^\circ(\text{react.}) = \sum_{i(\text{products})} n_i E_{TOT,i} - E_{TOT}(\text{react.})$, where E_{TOT} is the computed total electronic energy (that is zero-point energy corrected for the molecular species) and n_i is the stoichiometric coefficient of the i th product. From the computed binding energies it is then straightforward to obtain the enthalpies of formation at 0 K ($\Delta_f H_0^\circ$) of the species using the equation $\Delta_f H_0^\circ(\text{react.}) = \sum_{i(\text{products})} n_i \Delta_f H_0^\circ(i) - \Delta_{at}H_0^\circ(\text{react.})$, where $\Delta_f H_0^\circ$ of the products are experimental values taken from the JANAF tables.³³ For cations the atomization reaction is defined by Gurvich et al.³⁴ as $C_xH_yO_{(g)}^+ + e^- \rightarrow xC_{(g)} + yH_{(g)} + O_{(g)}$. Therefore, $\Delta_{at}H_0^\circ(C_xH_yO_{(g)}^+)$ can be calculated (using the electron convention)³⁵ as $\Delta_{at}H_0^\circ(\text{cation}) = \sum_{i(\text{products})} n_i E_{TOT,i} - E_{TOT}(\text{cation})$, and $\Delta_f H_0^\circ(C_xH_yO_{(g)}^+)$ as $\Delta_f H_0^\circ(\text{cation}) = \sum_{i(\text{products})} n_i \Delta_f H_0^\circ(i) - \Delta_{at}H_0^\circ(\text{cation})$. All the values are reported in Table 1. An estimated total uncertainty of 10 kJ mol^{-1} is chosen for the

SCHEME 1



SCHEME 2



calculated thermodynamic quantities, based on the experimental errors and computational accuracy of $4\text{--}5\text{ kJ mol}^{-1}$.²⁵

To test the reliability of the computed thermodynamic quantities obtained combining the experimental JANAF data with the CBS-QB3 energetics, we compare the experimentally known AIE and enthalpy of formation at 0 K of cyclopentanone with the calculated values. The CBS-QB3 AIE (9.29 eV) matches the experimental AIE of $9.26(\pm 0.01)\text{ eV}$ ²⁸ very well. There are three experimental determinations of $\Delta_f H_{298}^\circ(\text{c-C}_5\text{H}_8=\text{O})$ ranging from $-197.4(\pm 1.3)\text{ kJ mol}^{-1}$ ³⁶ to $-193.0(\pm 1.8)$

kJ mol^{-1} ,³⁷ which reported to 0 K become -171 to -167 kJ mol^{-1} , respectively. The CBS-QB3 $\Delta_f H_0^\circ$ of $-166(\pm 10)\text{ kJ mol}^{-1}$ is in good agreement with the experimental results within the computed uncertainty.

Finally, the isomeric species observed in the present system may shed some light on the oxidation chemistry of cyclopentene. Although the chemistry of peroxy radicals plays an important role at low temperature ($\leq 800\text{ K}$),^{38–40} only a higher temperature ($\geq 900\text{ K}$) mechanism for cyclopentene oxidation has been reported.^{41,42} In general, addition of O_2 to any of the three

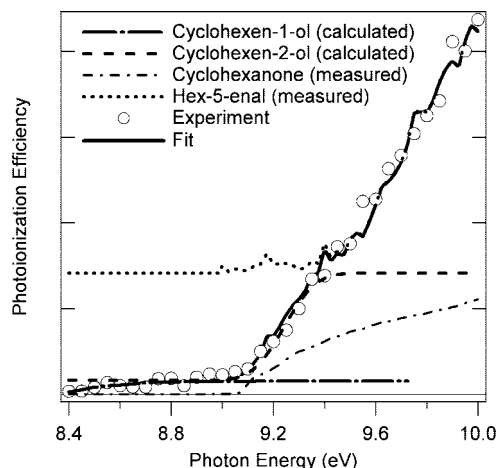


Figure 3. The best-fit overall Franck–Condon PIE curve (solid line) superimposed on the experimental PIE curve of m/z 98 isomers ($C_6H_{10}O$). The Franck–Condon envelopes for ionization of the individual isomers are also plotted separately to show the schematic decomposition of the best fit. The cyclohexanone PIE is shown for reference; its contribution to the best fit is very small.

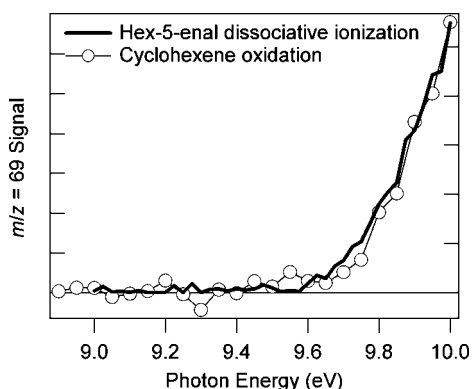


Figure 4. PIE curve of m/z 69 observed as a product of the OH-initiated oxidation of cyclohexene compared with the measured dissociative ionization photoionization efficiency spectrum for m/z 69 from hex-5-enal.

possible cyclopentenyl radicals that can be formed from H abstraction from cyclopentene—1-*c*- C_5H_7 (“vinylic radical”), 2-*c*- C_5H_7 (“allylic radical”), or 3-*c*- C_5H_7 (“alkylic radical”)—proceeds with the formation of peroxy radicals that can isomerize to hydroperoxyalkenyl ($Q'OOH$) radicals and dissociate into various products. Especially at low temperature, peroxy radicals are also likely to be formed by addition of OH to the double bond in cyclopentene and subsequent addition of O_2 . The resulting hydroxycyclopentylperoxy radical may eliminate HO_2 , leading to either of the two cyclopentenol isomers observed here or conceivably to *cis*-1,2-epoxycyclopentane, or it may form any of four possible epoxycyclopentanol isomers by elimination of OH, according to Scheme 2.

The *cis*-1,2-epoxycyclopentane isomer would likely not be detected here because the highest photon energy of 10 eV used in the present experiments is very close to its computed adiabatic ionization energy. On the other hand, according to the CBS-QB3 computations three of the four possible epoxycyclopentanols (1,2-epoxycyclopentanol, 2,4-epoxycyclopentanol, and 2,5-epoxycyclopentanol) change their structure substantially upon photoionization, opening the five-member ring, thus making their detection difficult due to poor Franck–Condon factors. Only 2,3-epoxycyclopentanol retains the C_5 ring structure, with an elongated C_α – $C(O)$ bond. This product is not

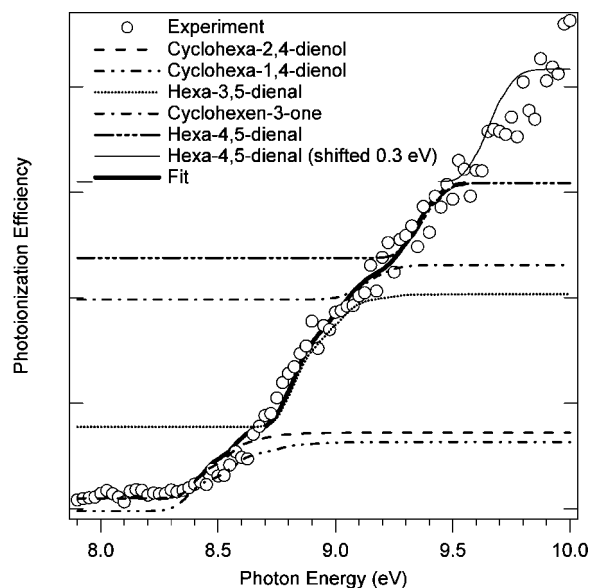


Figure 5. The best-fit overall Franck–Condon PIE curve (bold solid line) superimposed on the experimental PIE curve of m/z 96 isomers (C_6H_8O). The single electronic transitions of the isomers are also plotted separately (dotted lines) to show the schematic decomposition of the best fit. The thin solid line is the hexa-4,5-dienal curve displaced by the 0.3 eV gap between the two highest energy occupied molecular orbitals, and represents a zero-order estimate of possible ionization to the first excited state of the hexa-4,5-dienal cation.

detected in the present experiments, but may contribute at higher temperature where dissociation of the peroxy radicals is more rapid.

Cyclohexene and Cyclohexa-1,4-diene Oxidation. The OH-initiated oxidation of cyclopentene yields identifiable C_3H_8O products consistent with the mechanism in Scheme 1. Similar experiments on OH-initiated oxidation of the C_6 cyclic alkenes cyclohexene and 1,4-cyclohexadiene, however, show a more complex picture. Figure 3 shows the $C_6H_{10}O$ photoionization efficiency spectrum from OH-initiated cyclohexene oxidation. The signal below 9 eV is attributable to cyclohexen-1-ol, and the sharp onset near 9.1 eV can be fit by the calculated photoionization efficiency of cyclohexen-2-ol, with a possible very small contribution from cyclohexanone, the *keto* isomer of cyclohexen-1-ol. The cyclohexen-2-ol contribution is approximately $6(\pm 2)$ times that of the cyclohexen-1-ol, using once again the empirical method of Bobeldijk et al.³² to estimate relative cross sections. In contrast to the cyclopentene oxidation, which is dominated by cyclic products, at higher photon energy the m/z 98 product spectrum of cyclohexene oxidation exhibits contributions consistent with the linear isomer hex-5-enal ($CH_2=CHCH_2CH_2CH_2CHO$), whose photoionization efficiency spectrum and absolute photoionization cross section have been measured in connection with other (unpublished) experiments designed to probe product formation in cyclohexane oxidation. This isomer is a known product of the reaction of cyclohexyl radical with O_2 ,⁴³ and its formation in the present system suggests that ring-opening is a substantially more prominent pathway for oxidation of unsaturated cyclic C_6 hydrocarbons. Using the photoionization cross sections observed for cyclohexene and hex-5-enal, the observed hex-5-enal represents approximately 10% of the total cyclohexene that was removed in the reaction, and some four times the contribution of the cyclic species. The presence of hex-5-enal is supported by observation in the product spectrum of its dissociative ionization product at m/z 69, as shown in Figure 4. The relative amplitudes of the

m/z 69 and 98 species are, however, significantly different in the present product spectrum than in the measured spectrum of hex-5-enal. In fact, the amplitude of the m/z 69 cation signal suggests a contribution nearly three times larger than that implied by the parent m/z 98 amplitude. It is possible that some other product also contributes at m/z 69.

The OH-initiated oxidation of cyclohexa-1,4-diene has also been investigated, and the photoionization efficiency spectrum for the m/z 96 product (C_6H_8O) is displayed in Figure 5. The identification of the C_6H_8O isomers is somewhat more complex than that of the compounds discussed earlier; the cyclohexa-1,4-dienol or cyclohexa-2,4-dienol products of OH addition followed by α or γ H atom elimination can be discerned at low photon energy. The similarity of the calculated PIE curves for these two species makes them impossible to clearly distinguish. The best fit to the observed spectrum has no contribution from the enol (cyclohexa-1,4-dienol). However, a fit with the cyclohexa-2,4-dienol isomer held at zero, with its contribution therefore replaced by the enol, yields a χ^2 value that is only about 10% higher. The ring-opening product from 1,4-cyclohexadiene oxidation that is analogous to hex-5-enal formation in the cyclohexene system is hexa-3,5-dienal ($CH_2=CHCH=CH-CH_2CHO$); the product spectrum from OH-initiated oxidation of 1,4-cyclohexadiene appears to show a substantial contribution of this isomer at 8.8 eV, with an overall contribution similar to that of hex-5-enal in the cyclohexene system. The decomposition into as complex a set of isomers as depicted in Figure 5 must be regarded as somewhat qualitative, but some conclusions of the analysis are rather robust. For example, an extensive search for possible ring-containing carriers near 8.8 eV ionization energy was fruitless (Table 2), adding substantially to the confidence that ring-opening is a prominent pathway. In analogy with cyclopentene and cyclohexene OH oxidation, the *keto* isomer of cyclohexa-1,4-dienol, cyclohexen-3-one, is at best weakly present in the PIE curve with a calculated AIE of 9.02 eV. The calculated photoelectron spectrum of cyclohexen-3-one does not present an extended vibrational progression, and this is inconsistent with the PIE curve of m/z 96 (Figure 5), in which the ion signal keeps rising after 9.3 eV. From computation of ionization energies of plausible isomers, hexa-4,5-dienal, an additional ring-opening product was found to have the appropriate AIE of 9.28 eV. Moreover, the second highest occupied molecular orbital in hexa-4,5-dienal is 0.3 eV lower in energy than the highest occupied molecular orbital. Within a Koopman's theorem approximation the term energy for the first excited electronic state of the hexa-4,5-dienal cation can therefore be estimated as approximately 0.3 eV. This result may extend the PIE envelope for hexa-4,5-dienal as qualitatively depicted in Figure 5 (of course the true Franck-Condon factors for the excited cation state will be different).

There is a clear difference between the isomeric C_5H_8O products in cyclopentene OH-initiated oxidation and the $C_6H_{10}O$ and C_6H_8O products from oxidation of cyclohexene and 1,4-cyclohexadiene, respectively. One speculation is that the difference in product distributions, with cyclopentene oxidation lacking the linear aldehyde product, is that the ring-opening mechanism may involve a bicyclic transition state (TS). This TS would consist of 3- and 4-member rings for cyclopentene and 3- and 5-member rings for both cyclohexene and 1,4-cyclohexadiene. From this assumption it is then simple to recognize that the TS with the 4-member ring is more destabilized due to higher ring strain than the TS with the 5-member ring. This stronger ring strain may be sufficient to make the pathway for the ring-opening product of cyclopentene

prohibitive under the present experimental conditions. However, the details of the ring-opening channel are not known, and future isotopically labeled experiments may be useful to unravel the mechanism.

Conclusions

The isomeric products from OH-initiated oxidation of cyclopentene, cyclohexene, and 1,4-cyclohexadiene have been investigated by tunable-synchrotron photoionization mass spectrometry. Formation of unsaturated cyclic alcohols is evident in all three systems. The measured adiabatic ionization energy of 1-*c*- C_5H_7OH is 8.4(\pm 0.1) eV, and that of 2-*c*- C_5H_7OH is 9.5(\pm 0.1) eV. Ring-opening channels are prominent in the oxidation of the six-carbon species but absent in the cyclopentene oxidation.

Acknowledgment. We thank Howard Johnsen for technical assistance and Darryl Sasaki for the synthesis of hex-5-enal. This work is supported by the Division of Chemical Sciences, Geosciences, and Biosciences, the Office of Basic Energy Sciences, the U.S. Department of Energy. Sandia is a multi-program laboratory operated by Sandia Corporation, a Lockheed Martin Company, for the National Nuclear Security Administration under contract DE-AC04-94-AL85000. The Advanced Light Source is supported by the Director, Office of Science, Office of Basic Energy Sciences, Materials Sciences Division, of the U.S. Department of Energy under Contract No. DE-AC02-05CH11231 at Lawrence Berkeley National Laboratory.

References and Notes

- (1) Taatjes, C. A.; Hansen, N.; McLroy, A.; Miller, J. A.; Senosiain, J. P.; Klippenstein, S. J.; Qi, F.; Sheng, L.; Zhang, Y.; Cool, T. A.; Wang, J.; Westmoreland, P. R.; Law, M. E.; Kasper, T.; Kohse-Hoinghaus, K. *Science* **2005**, *308*, 1887.
- (2) Taatjes, C. A.; Hansen, N.; Miller, J. A.; Cool, T. A.; Wang, J.; Westmoreland, P. R.; Law, M. E.; Kasper, T.; Kohse-Hoinghaus, K. *J. Phys. Chem. A* **2006**, *110*, 3254.
- (3) Ghigo, G.; Tonachini, G. *J. Am. Chem. Soc.* **1998**, *120*, 6753.
- (4) Atkinson, R. *J. Phys. Chem. Ref. Data* **1994**, R1.
- (5) Hansen, N.; Klippenstein, S. J.; Miller, J. A.; Wang, J.; Cool, T. A.; Law, M. E.; Westmoreland, P. R.; Kasper, T.; Kohse-Hoinghaus, K. *J. Phys. Chem. A* **2006**, *110*, 4376.
- (6) Hansen, N.; Kasper, T.; Klippenstein, S. J.; Westmoreland, P. R.; Law, M. E.; Taatjes, C. A.; Kohse-Hoinghaus, K.; Wang, J.; Cool, T. A. *J. Phys. Chem. A* **2007**, *111*, 4081.
- (7) Gomez, A.; Sidebotham, G.; Glassman, I. *Combust. Flame* **1984**, *58*, 45.
- (8) McEnally, C. S.; Pfefferle, L. D. *Combust. Sci. Technol.* **1998**, *131*, 323.
- (9) Hatakeyama, S.; Ohno, M.; Weng, J. H.; Takagi, H.; Akimoto, H. *Environ. Sci. Technol.* **1987**, *21*, 52.
- (10) Grosjean, D.; Friedlander, S. K. *Adv. Environ. Sci. Technol.* **1980**, *9*, 435.
- (11) Cool, T. A.; Nakajima, K.; Mostefaoui, T. A.; Qi, F.; McLroy, A.; Westmoreland, P. R.; Law, M. E.; Poisson, L.; Peterka, D. S.; Ahmed, M. *J. Chem. Phys.* **2003**, *119*, 8356.
- (12) Turner, B. E.; Apponi, A. *J. Astrophys. J.* **2001**, *561*, L207.
- (13) Archibald, A. T.; McGillen, M. R.; Taatjes, C. A.; Percival, C. J.; Shallcross, D. E. *Geophys. Res. Lett.* **2007**, *34*, L21801.
- (14) Saito, S. *Chem. Phys. Lett.* **1976**, *42*, 399.
- (15) Hay, J. M.; Lyon, D. *Nature* **1967**, *216*, 790.
- (16) Bouma, W. J.; Macleod, J. K.; Radom, L. *J. Am. Chem. Soc.* **1979**, *101*, 5540.
- (17) Rodler, M. *J. Mol. Spectrosc.* **1985**, *114*, 23.
- (18) Matti, G. Y.; Osman, O. I.; Upham, J. E.; Suffolk, R. J.; Kroto, H. W. *J. Electron Spectrosc. Relat. Phenom.* **1989**, *49*, 195.
- (19) Osborn, D. L.; Zou, P.; Johnsen, H.; Hayden, C. C.; Taatjes, C. A.; Knyazev, V. D.; North, S. W.; Peterka, D. S.; Ahmed, M.; Leone, S. R. *Rev. Sci. Instrum.* **2008**, *79*, 104103.
- (20) Sinha, M. P.; Wadsworth, M. *Rev. Sci. Instrum.* **2005**, *76*, 025103.
- (21) Vallerga, J. V.; Siegmund, O. H. W. *Nucl. Instrum. Methods Phys. Res. A* **2000**, *442*, 159.
- (22) Meloni, G.; Selby, T. M.; Goulay, F.; Leone, S. R.; Osborn, D. L.; Taatjes, C. A. *J. Am. Chem. Soc.* **2007**, *129*, 14019.

- (23) Frisch, M. J.; Trucks, G. W.; Schlegel, H. B.; Scuseria, G. E.; Robb, M. A.; Cheeseman, J. R.; Montgomery, J. A., Jr.; Vreven, T.; Kudin, K. N.; Burant, J. C.; Millam, J. M.; Iyengar, S. S.; Tomasi, J.; Barone, V.; Mennucci, B.; Cossi, M.; Scalmani, G.; Rega, N.; Petersson, G. A.; Nakatsuji, H.; Hada, M.; Ehara, M.; Toyota, K.; Fukuda, R.; Hasegawa, J.; Ishida, M.; Nakajima, T.; Honda, Y.; Kitao, O.; Nakai, H.; Klene, M.; Li, X.; Knox, J. E.; Hratchian, H. P.; Cross, J. B.; Bakken, V.; Adamo, C.; Jaramillo, J.; Gomperts, R.; Stratmann, R. E.; Yazyev, O.; Austin, A. J.; Cammi, R.; Pomelli, C.; Ochterski, J. W.; Ayala, P. Y.; Morokuma, K.; Voth, G. A.; Salvador, P.; Dannenberg, J. J.; Zakrzewski, V. G.; Dapprich, S.; Daniels, A. D.; Strain, M. C.; Farkas, O.; Malick, D. K.; Rabuck, A. D.; Raghavachari, K.; Foresman, J. B.; Ortiz, J. V.; Cui, Q.; Baboul, A. G.; Clifford, S.; Cioslowski, J.; Stefanov, B. B.; Liu, G.; Liashenko, A.; Piskorz, P.; Komaromi, I.; Martin, R. L.; Fox, D. J.; Keith, T.; Al-Laham, M. A.; Peng, C. Y.; Nanayakkara, A.; Challacombe, M.; Gill, P. M. W.; Johnson, B.; Chen, W.; Wong, M. W.; Gonzalez, C.; Pople, J. A. *Gaussian 03*, Revision C.02; Gaussian, Inc.: Wallingford, CT, 2004.
- (24) Montgomery, J. A.; Frisch, M. J.; Ochterski, J. W.; Petersson, G. A. *J. Chem. Phys.* **1999**, *110*, 2822.
- (25) Montgomery, J. A.; Frisch, M. J.; Ochterski, J. W.; Petersson, G. A. *J. Chem. Phys.* **2000**, *112*, 6532.
- (26) Durig, J. R.; Coulter, G. L.; Wertz, D. W. *J. Mol. Spectrosc.* **1968**, *27*, 285.
- (27) Erlandsson, G. *J. Chem. Phys.* **1954**, *22*, 563.
- (28) Lias, S. G. *Ionization Energy Evaluation*; National Institute of Standards and Technology: Gaithersburg, MD 2005.
- (29) Ervin, K. M.; Ramond, T. M.; Davico, G. E.; Schwartz, R. L.; Casey, S. M.; Lineberger, W. C. *J. Phys. Chem. A* **2001**, *105*, 10822.
- (30) Ervin, K. M. *PESCAL*, Fortran program; University of Nevada: Reno, 2004.
- (31) Duschinsky, F. *Acta Physicochim. URSS* **1937**, *7*, 551.
- (32) Bobeldijk, M.; Zande, W. J. v. d.; Kistemaker, P. G. *Chem. Phys.* **1994**, *179*, 125.
- (33) *NIST-JANAF Thermochemical Tables*, 4th ed.; American Chemical Society: Washington, DC, 1998.
- (34) *Thermodynamic Properties of Individual Substances*; Hemisphere: New York, 1991; Vol. 1.
- (35) Ervin, K. M. *Chem. Rev.* **2001**, *101*, 391.
- (36) Wiberg, K. B.; Crocker, L. S.; Morgan, K. M. *J. Am. Chem. Soc.* **1991**, *113*, 3447.
- (37) Cox, J. D.; Pilcher, G. *Thermochemistry of Organic and Organometallic Compounds*; Academic Press: New York, 1970.
- (38) Benson, S. W. *J. Am. Chem. Soc.* **1965**, *87*, 972.
- (39) Wallington, T. J.; Dagaut, P.; Kurylo, M. J. *Chem. Rev.* **1992**, *92*, 667.
- (40) Finlayson-Pitts, B. J.; Pitts, J. N. *Science* **1997**, *276*, 1045.
- (41) Gueniche, H. A.; Glaude, P. A.; Fournet, R.; Battin-Leclerc, F. *Combust. Flame* **2008**, *152*, 245.
- (42) Yahyaoui, M.; Hakka, M. H.; Glaude, P. A.; Battin-Leclerc, F. *Int. J. Chem. Kinet.* **2008**, *40*, 25.
- (43) Knepp, A. M.; Meloni, G.; Jusinski, L. E.; Taatjes, C. A.; Cavallotti, C.; Klippenstein, S. J. *Phys. Chem. Chem. Phys.* **2007**, *9*, 4315.

JP808015F